Contemporary Engineering Sciences, Vol. 5, 2012, no. 9, 413 - 426

L-Band SiGe HBT Frequency-Tunable Dual-Bandpass or Dual-Bandstop Differential Amplifiers Using Varactor-Loaded, Stacked LC-Resonators

Kazuyoshi Sakamoto

1-1-25 Tsujido-Nishikaigan,
Fujisawa, Kanagawa, 251-8511 Japan

Yasushi Itoh

1-1-25 Tsujido-Nishikaigan,
Fujisawa, Kanagawa, 251-8511 Japan
itohy@center.shonan-it.ac.jp

Abstract

L-band SiGe HBT frequency-tunable dual-bandpass or dual-bandstop differential amplifiers have been developed for the next generation adaptive and/or reconfigurable wireless radios. Varactor-loaded, stacked LC-resonators are used in the output circuit of differential amplifiers for realizing dual-bandpass responses as well as in the series feedback circuit for dual-bandstop responses. The varactor-loaded, stacked LC-resonator can provide bandpass or bandstop responses for multiple frequencies and the resonant frequencies can be tuned independently. With the use of the varactor-loaded, dual-band resonator in the output circuit of 0.35μm SiGe HBT differential amplifiers, the lower bandpass frequency can be varied from 0.6 to 1 GHz with a fixed upper bandpass frequency of 1.12 GHz. Meanwhile, the upper bandpass frequency can be varied from 0.69 to 1.07 GHz for a fixed lower bandpass frequency of 0.62 GHz. The dual-band gain was 9 to 13 dB over the whole frequency band. In addition, with the use of the varactor-loaded, dual-band resonator in the series feedback circuit of 0.35μm SiGe HBT differential amplifiers, the lower bandstop frequency can be varied from 0.87 to 1.28 GHz with a fixed upper bandstop frequency of 1.55 GHz.

Meanwhile, the upper bandstop frequency can be varied from 0.97 to 1.54 GHz with a fixed lower bandstop frequency of 0.87 GHz. The maximal dual-band rejection of gain was 16 dB. The varactor-loaded, stacked resonator presented in this paper is expected to be a key circuit technology for realizing bandpass or bandstop responses for multiple frequencies in the next generation adaptive and/or reconfigurable wireless transceivers.

Keywords: amplifier, differential, microwave, frequency-tunable, SiGe HBT, varactor, LC-resonator, dual-band

1 Introduction

After the 3G and 4G wireless communication systems are introduced, the evolution of wireless radios including the adaptive, reconfigurable multi-standard transceivers is accelerated [1], [2]. The frequency spectrum becomes also wider from the traditional L/S-band to the upcoming C/X-band to meet a wide range of date rates over several frequency bands of wireless radios [3]. Since the active radios are collocated in both frequency and space, the interference and image rejection become a crucial issue [4]. In the multi-band and multi-mode receiving operations, the image signals actually drop into the current frequency band, necessarily leading to time-frequency collisions and interferences. In order to meet these requirements, various types of multi-band amplifiers with bandpass or bandstop responses have been actively researched and developed by several companies in the world. Most of the multi-band amplifiers with bandpass responses have focused on the concurrent amplification [5], including wideband matching [6], dual-band matching with a fixed frequency [7] and single-band matching with a tunable frequency [8]. On the other hand, various types of multi-band amplifiers with bandstop responses have been reported, including active interference canceller [4], image rejection LNA [9], [10] and frequency-agile absorptive bandstop filter [11]. As a novel design method for multiple bandpass or bandstop performance, the authors have presented the stacked LC-resonator in the output circuit for multiple bandpass responses [12], [13] or in the series feedback circuit for multiple bandstop responses [14]. The bandpass or bandstop amplifier in [12], [13], however, had a fixed frequency as well as the bandstop amplifier in [14] has used an active load in the LC-resonator for a tunable rejection level, which seriously degraded gain.

To address this problem, varactor diodes are loaded in stacked LC-resonators for realizing frequency-tunable bandpass or bandstop performances at multiple frequencies. In addition, the active load was eliminated from LC-resonators to improve gain and Q-factor. In an application of the front-end circuit in the next generation adaptive and/or reconfigurable wireless radios, noise figure and IIP_3 performance have been evaluated. In order to ensure the usefulness of the varactor-loaded, stacked LC-resonators, L-band SiGe HBT differential amplifiers with dual-bandpass or dual-bandstop responses have been designed, fabricated and tested.

2 Varactor-loaded, Stacked LC-Resonators

A schematic diagram of the differential amplifier with the output circuit Z_L and the series feedback circuit Z_S is shown in Fig. 1. The gain G can be approximated as the following equation:

$$G = \left| \frac{Z_L}{Z_S} \right| \tag{1}$$

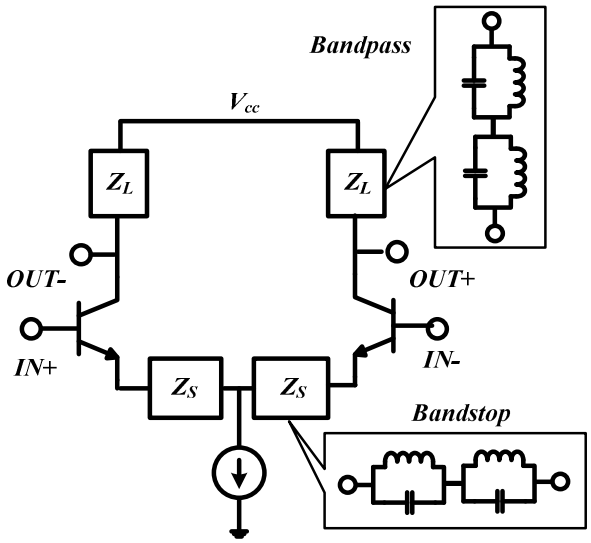

Fig. 1 Schematic diagram of the differential amplifier with the output circuit Z_L and the series feedback circuit Z_S

The maximal gain is obtained for an open-circuited Z_L or a short-circuited Z_S. Meanwhile, the minimal gain is obtained for a short-circuited Z_L or an open-circuited Z_S. From the bias-feeding point of view, an open-circuited Z_L or Z_S were finally chosen for bandpass or bandstop responses, respectively.

A schematic diagram of the varactor-loaded, stacked dual-band resonator is shown Fig. 2. Two parallel LC circuits of (L_1, C_1+C_{V1}) and (L_2, C_2+C_{V2}) are cascaded in series. C_C is a decoupling capacitor with a large capacitance value and thus can be assumed as short. This resonator provides dual bandpass frequencies (f_1, f_2) and single bandstop frequency (f_3). If it is assumed that $L_1(C_1+C_{V1}) > L_2(C_2+C_{V2})$, then f_1, f_2 and f_3 are given as follows: f_3 is necessarily sandwiched between f_1 and f_2, that is, $f_1 < f_3 < f_2$.

$$f_1 = \frac{1}{2\pi\sqrt{L_1(C_1 + C_{V1})}} \tag{2}$$

$$f_2 = \frac{1}{2\pi\sqrt{L_2(C_2 + C_{V2})}} \tag{3}$$

$$f_3 = \frac{1}{2\pi}\sqrt{\frac{1/L_1 + 1/L_2}{C_1 + C_{V1} + C_2 + C_{V2}}} \tag{4}$$

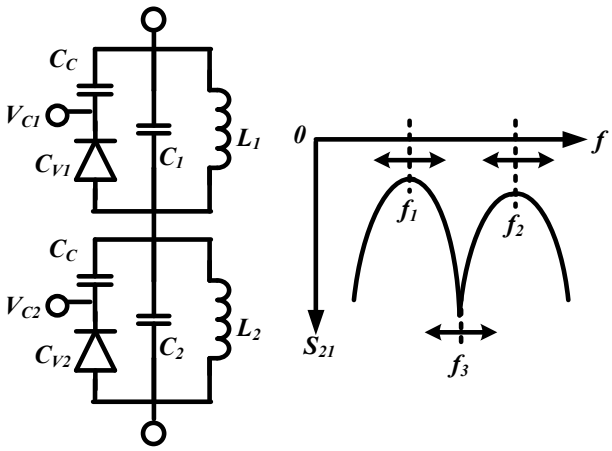

Fig. 2 Schematic diagram of the varactor-loaded, stacked dual-band resonator

f_1, f_2 and f_3 are calculated by using Eqs. (2), (3) and (4). The calculated results are shown in Fig. 3 for a variable C_{V2} and a fixed C_{V1} as well as in Fig. 4 for a variable C_{V1} and a fixed C_{V2}. The element values are also shown in Figs. 3 and 4. Si varactor diodes with a capacitance ratio of 2.5:1 (C_{2V}=6pF and C_{10V}=15pF) were used. It is clearly shown in Figs. 3 and 4 that f_1 and f_2 can be independently varied.

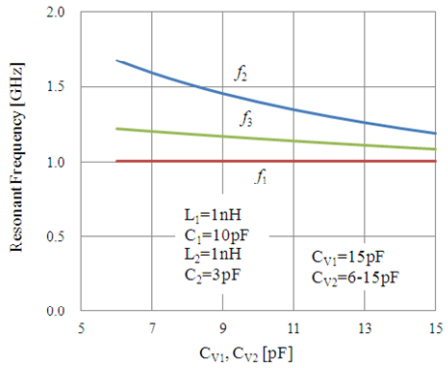

Fig. 3 Calculated f_1, f_2 and f_3 for a variable C_{V2} and a fixed C_{V1}

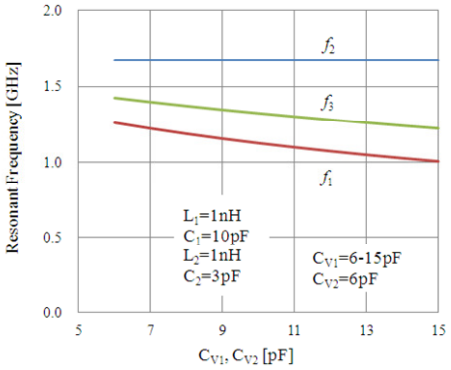

Fig. 4 Calculated f_1, f_2 and f_3 for a variable C_{V1} and a fixed C_{V2}

Based on the calculated results, the insertion loss (S_{21}) of the stacked dual-band resonator of Fig. 2 was measured and plotted in Fig. 5 for a variable V_{C2} and a fixed V_{C1} as well as in Fig. 6 for a variable V_{C1} and a fixed V_{C2}, respectively. V_{C1} and V_{C2} are a control voltage of the varactor diode. It is also clearly shown that f_1 and f_2 can be independently varied. The measured resonant frequencies of f_1 and f_2 are plotted in Fig. 7. f_1 moves from 0.61 to 1.15 GHz for a fixed f_2 of 1.39 GHz. In addition, f_2 moves from 0.63 to 1.39 GHz for a fixed f_1 of 0.62 GHz.

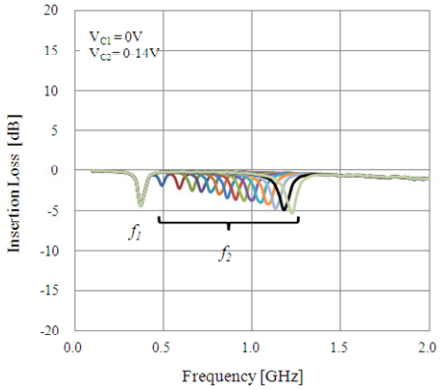

Fig. 5 Measured insertion loss for a variable V_{C2} and a fixed V_{C1}

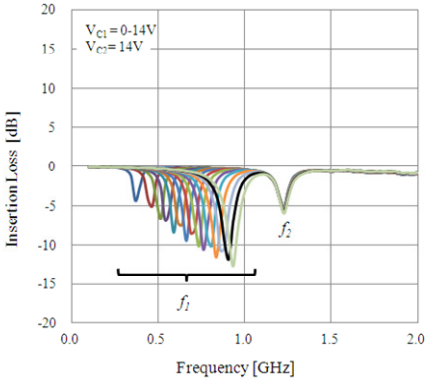

Fig. 6 Measured insertion loss for a variable V_{C1} and a fixed V_{C2}

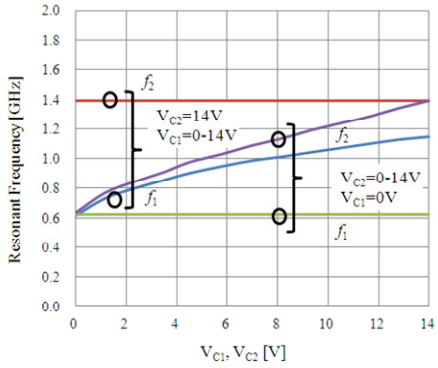

Fig. 7 Measured resonant frequencies of f_1 and f_2

3 Dual-Bandpass Differential Amplifiers

A schematic diagram of the L-band SiGe HBT frequency-tunable dual-bandpass differential amplifier is shown in Fig. 8. The varactor-loaded, stacked dual-band resonator of Fig. 2 is employed in the output circuit Z_L to achieve dual-bandpass responses. Contrary to the references [12], [13], a varactor diode is connected in parallel with LC-resonators to provide a frequency-tunable capability. A cascode connection of HBTs is used to achieve high gain as well as variable gain. V_{CC} and V_{B2} are a supply voltage and a control voltage of the 2nd base bias, respectively. The circuit element values are listed in Table 1.

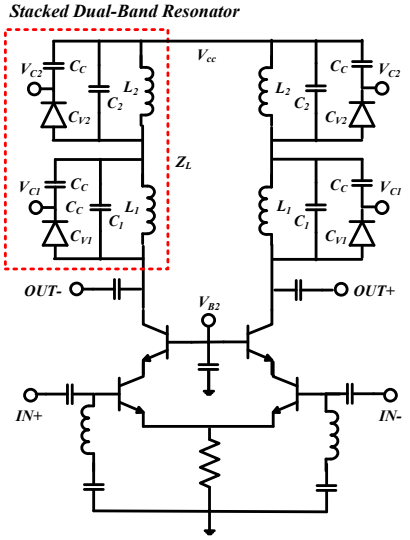

Fig. 8 Schematic diagram of the L-band SiGe HBT frequency-tunable dual-bandpass differential amplifier

Table 1 Circuit element values

Element	Value
L_1	1nH
L_2	1nH
C_1	10pF
C_2	3pF
C_{V1}	6-15pF
C_{V2}	6-15pF
C_C	1000pF

A photograph of the L-band SiGe HBT frequency-tunable dual-bandpass differential amplifier is shown in Fig. 9. The amplifier was fabricated on the FR-4 substrate with a dielectric constant of 4.5. 1005-type chip resistors, capacitors, and

inductors are mounted on the substrate by soldering. A surface mount type of the SiGe HBT with an f_t of around 25 GHz and the Si varactor diode with a capacitance ratio of 2.5:1 are employed. The circuit size is 16 x 16 x 1.2 mm^3.

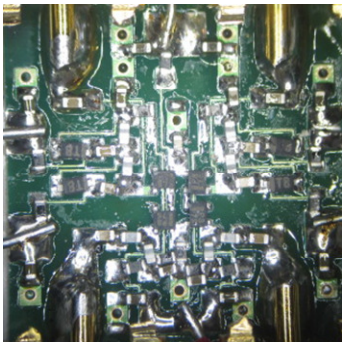

16 x 16 x 1.2 mm^3

Fig. 9 Photograph of the L-band SiGe HBT frequency-tunable dual-bandpass differential amplifier

Measured gains of the frequency-tunable dual-bandpass differential amplifier are shown in Fig. 10 for a variable V_{C2} (C_{V2}) and a fixed V_{C1} (C_{V1}) as well as in Fig. 11 for a variable V_{C1} (C_{V1}) and a fixed V_{C2} (C_{V2}). In Fig. 11, the lower bandpass frequency was varied from 0.6 to 1.0 GHz with a fixed upper bandpass frequency of 1.12 GHz. On the other hand, the upper bandpass frequency can be varied from 0.69 to 1.07 GHz for a fixed lower bandpass frequency of 0.62 GHz in Fig. 10. The dual-band gain was 9 to 13 dB over the whole frequency band. The bias conditions of V_{CC}, V_{B2}, V_{C1} and V_{C2} are also shown in Figs. 10 and 11. A collector current was around 8mA. Another gain peak appears above 1.5 GHz in Figs. 10 and 11, which is due to the parasitic reactance of the circuit elements.

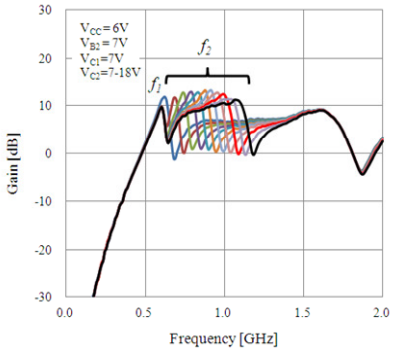

Fig. 10 Measured gains of the frequency-tunable dual-bandpass differential amplifier for a variable V_{C2} (C_{V2}) and a fixed V_{C1} (C_{V1})

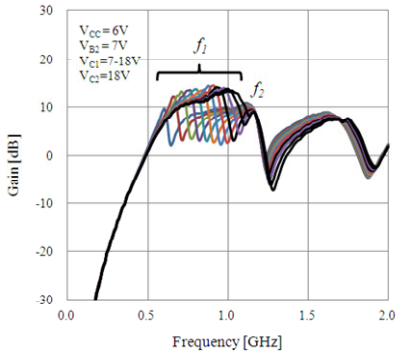

Fig. 11 Measured gains of the frequency-tunable dual-bandpass differential amplifier for a variable V_{C1} (C_{V1}) and a fixed V_{C2} (C_{V2})

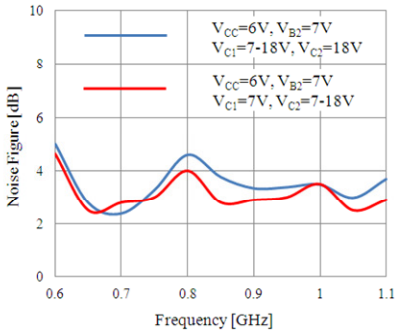

Fig. 12 Measured noise figures for a fixed V_{C1} (C_{V1}) and a variable V_{C2} (C_{V2}) as well as for a variable V_{C1} (C_{V1}) and a fixed V_{C2} (C_{V2})

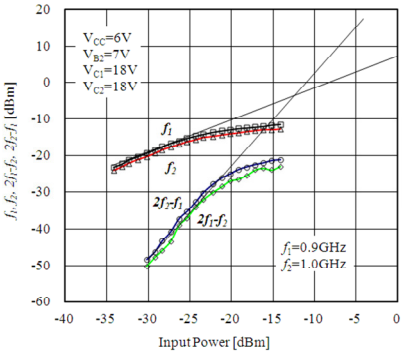

Fig. 13 Measured IIP_3 performances of the frequency-tunable dual-bandpass differential amplifier

Measured noise figures for a fixed V_{C1} (C_{V1}) and a variable V_{C2} (C_{V2}) as well as for a variable V_{C1} (C_{V1}) and a fixed V_{C2} (C_{V2}) are shown in Fig. 12. Noise figures were measured at a frequency providing a maximal gain for both bias conditions. The minimal noise figure was 2.4 dB for both bias conditions. IIP_3 was measured with two tones of 0.9 and 1 GHz and plotted in Fig. 13. Bias conditions are also shown in Fig. 13. The minimal IIP_3 was -12.5 dBm.

4 Dual-Bandstop Differential Amplifiers

A schematic diagram of the L-band SiGe HBT frequency-tunable dual-bandstop differential amplifier is shown in Fig. 14. The varactor-loaded, stacked dual-band resonator shown in Fig. 2 is employed in the series feedback circuit to achieve dual-bandstop responses. The circuit element values are listed in Table 2. In contrast to the reference [14], the active load (a variable resistor) was eliminated to improve gain and Q-factor. V_{CC} is a supply voltage as well as V_{C1} and V_{C2} are a control voltage of the varactor diode.

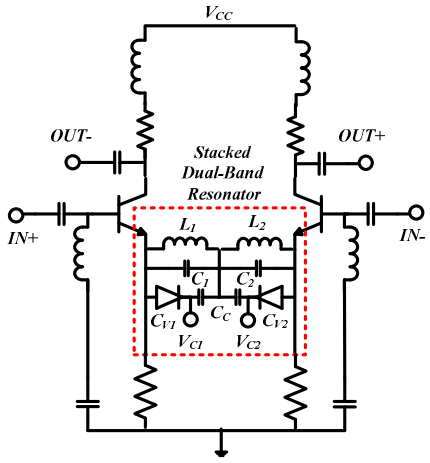

Fig. 14 Schematic diagram of the L-band SiGe HBT frequency-tunable dual-bandstop differential amplifier

Table 2 Circuit element values

Element	Value
L_1	1nH
L_2	1nH
C_1	10pF
C_2	3pF
C_{V1}	6-15pF
C_{V2}	6-15pF
C_C	1000pF

A photograph of the L-band SiGe HBT frequency-tunable dual-bandstop differential amplifier is shown in Fig. 15. The amplifier was fabricated on the FR-4 substrate with a dielectric constant of 4.5. 1005-type chip resistors, capacitors, and inductors are mounted on the substrate by soldering. A surface mount type of the SiGe HBT with an f_t of around 25 GHz and the Si varactor diode with a capacitance ratio of 2.5:1 are employed. The circuit size is 16 x 16 x 1.2 mm^3.

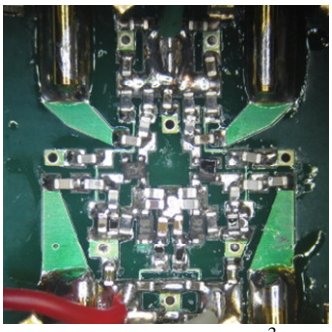

16 x 16 x 1.2 mm^3

Fig. 15 Photograph of the L-band SiGe HBT frequency-tunable dual-bandstop differential amplifier

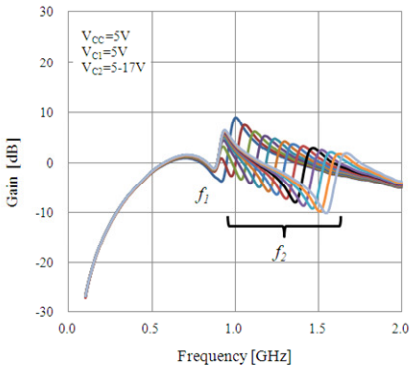

Fig. 16 Measured gains of the frequency-tunable dual-bandstop differential amplifier for a variable V_{C2} (C_{V2}) and a fixed V_{C1} (C_{V1})

Measured gains of the frequency-tunable dual-bandstop differential amplifier are shown in Fig. 16 for a variable V_{C2} (C_{V2}) and a fixed V_{C1} (C_{V1}) as well as in Fig. 17 for a variable V_{C1} (C_{V1}) and a fixed V_{C2} (C_{V2}). In Fig. 16, the upper bandstop frequency was varied from 0.97 to 1.54 GHz with a fixed lower bandstop frequency of 0.87 GHz. Meanwhile, the lower bandstop frequency can be varied from 0.87 to 1.28 GHz with a fixed upper bandstop frequency of 1.55 GHz in Fig. 17. The maximal dual-band rejection of gain was 16 dB. The bias

conditions for V_{CC}, V_{C1} and V_{C2} are also shown in Figs. 16 and 17. A collector current was around 8mA.

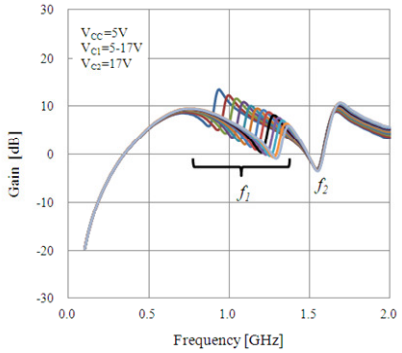

Fig. 17 Measured gains of the frequency-tunable dual-bandstop differential amplifier for a variable V_{C1} (C_{V1}) and a fixed V_{C2} (C_{V2})

Measured noise figures for a variable V_{C2} (C_{V2}) and a fixed V_{C1} (C_{V1}) as well as for a variable V_{C1} (C_{V1}) and a fixed V_{C2} (C_{V2}) are shown in Fig. 18. Noise figures were measured at a frequency providing a maximal gain for both bias conditions. The minimal noise figure was 3.55 dB for a fixed V_{C2} (C_{V2}) and a variable V_{C1} (C_{V1}) and 4.36 dB for a variable V_{C2} (C_{V2}) and a fixed V_{C1} (C_{V1}). IIP_3 was measured with two tones of 0.9 and 1 GHz and plotted in Fig. 19. Bias conditions are also shown in Fig. 19. The minimal IIP_3 was 0 dBm.

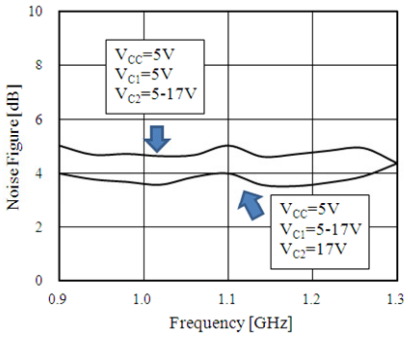

Fig. 18 Measured noise figures for a variable V_{C2} (C_{V2}) and a fixed V_{C1} (C_{V1}) as well as for a variable V_{C1} (C_{V1}) and a fixed V_{C2} (C_{V2})

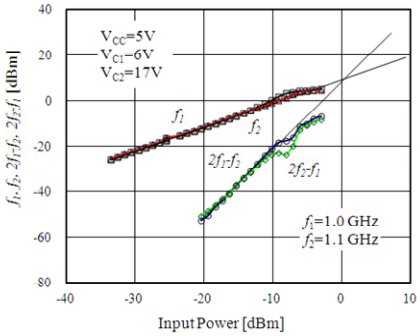

Fig. 19 Measured IIP_3 of the frequency-tunable dual-bandstop differential amplifier

5 Conclusions

The L-band SiGe HBT frequency-tunable dual-bandpass or dual-bandstop differential amplifiers using the varactor-loaded, stacked LC-resonators have been presented for the next generation adaptive and/or reconfigurable wireless radios. The varactor-loaded, stacked LC-resonator can provide bandpass or bandstop responses for multiple frequencies and the resonant frequencies can be tuned independently. With the use of the varactor-loaded, dual-band resonator in the output circuit of 0.35μm SiGe HBT differential amplifiers, it has been confirmed that the lower and upper bandpass frequencies can be varied independently. Meanwhile, with the use of the varactor-loaded, dual-band resonator in the series feedback circuit of 0.35μm SiGe HBT differential amplifiers, it has been also confirmed that the lower and upper bandstop frequencies can be varied independently. The frequency-tunable dual-bandpass or dual-bandstop amplifier presented in this paper is expected to greatly contribute to a miniaturization, low-cost and high performance of the current multi-band, multi-mode wireless transceivers for use in the next generation adaptive and/or reconfigurable wireless radios.

References

[1] A. R. Rofougaran, M. Rofougaran and A. Behzad, “Radios for Next-Generation Wireless Networks”, IEEE Microwave Magazine, 3(2005), 38-45.
[2] J. F. Luy, T. Muceller, T. Mack and A. Terzis, “Configurable RF Receiver Architectures”, IEEE Microwave Magazine, 3(2004), 75-82.
[3] G. R. Aiello and G. D. Rogerson, “Ultra-Wideband Wireless Systems”, IEEE Microwave Magazine, 6(2003), 36-48.

[4] A. Raghavan., E. Gebara, M. Tentzeris, J. Laskar, "An Active Interference Canceller for Multistandard Collocated Radio, IEEE MTT-S Digest, (2005), 723-726.
[5] H. Hashemi and A. Hajimiri, "Concurrent Multiband Low-Noise Amplifiers – Theory, Design, and Applications", IEEE Trans. MTT, 50(2002), 288-301.
[6] Y. T. Lin and S. S. Lu, "A 2.4/3.5/4.9/5.2/5.7-GHz concurrent multiband low noise amplifier using InGaP/ GaAs HBT Technology", IEEE Microwave and Wireless Component Letters, 10 (2004), 463-465.
[7] H. Nakajima, and M. Muraguchi, "Dual-Frequency Matching Technique and Its Application to an Octave-Band (30-60 GHz) MMIC Amplifier", IEICE Transaction on Electronics, 12(1997), 1614-1621.
[8] S. O. Yun and H. J. Yoo, "Multi-Standard CMOS Power Amplifier with Reconfigurable Matching Networks", IEICE Trans. Fundamentals Vol. E85-A/B/C/D, 1(2002), 1-7.
[9] W. Chen, S. Chang, G. Huang, Y. Jean, T. Yeh, "A Ku-Band Interference-Rejection CMOS Low-Noise Amplifier Using Current-Reused Stacked Common-Gate Topology", IEEE Microwave and Wireless Component Letters, 17(2007), 718-720.
[10] T. Nguyen, N. Oh, C. Cha, Y. Oh, G. Ihm, S. Lee, "Image-Rejection CMOS Low-Noise Amplifier Design Optimization Techniques", IEEE Transaction on Microwave Theory & Techniques, 53(2005), 538-545.
[11] D. Jachowski, "Compact, Frequency-Agile, Absorptive Bandstop Filters", IEEE MTT-S Digest, (2005), 513-516.
[12] Y. Itoh, "L-Band SiGe HBT Differential Amplifiers Using Stacked Parallel-Resonant Circuits", Contemporary Engineering Sciences, 1(2008), 127-138.
[13] M. Shirata, T. Shinohara, M. Sato, and Y. Itoh, "An L-Band SiGe HBT Differential Amplifier with Frequency and Rejection-Level Tunable, Multiple Stopband", International Journal of Microwave and Wireless Technologies, 1(2009), 285-292.
[14] Y. Itoh, T. Shinohara, M. Shirata, K. Sakamoto, "Eightfold-Band Differential SiGe HBT Amplifier Using Stacked LC-Tank Circuits", Proceeding of the Asia-Pacific Microwave Conference, (2008), A1-47.

Received: June, 2012